J. Sens. Sens. Syst., 4, 313–319, 2015
www.j-sens-sens-syst.net/4/313/2015/
doi:10.5194/jsss-4-313-2015

JSSS Journal of Sensors and Sensor Systems Open Access

Efficient thermal infrared emitter with high radiant power

T. Ott, M. Schossig, V. Norkus, and G. Gerlach
Institute for Solid-State Electronics, Technische Universität Dresden, 01062 Dresden, Germany

Correspondence to: T. Ott (tobias.ott@tu-dresden.de)

Received: 17 September 2015 – Accepted: 12 October 2015 – Published: 13 November 2015

Abstract. Sensitive and selective gas measurements are crucial for a large variety of applications, e.g., explosion protection. Optical gas detection is usually based on the gas' absorption of infrared radiation (IR). It is the leading technique in terms of accuracy, reliability, and economic efficiency. Since most gas measurements are made in the two wavelength ranges of (3 . . . 5) and (8 . . . 14) µm, a broadband IR source is necessary. In this paper, we report on a novel thermal IR emitter with high radiant power and a near-blackbody emission characteristic that can be modulated electrically. The layout of the IR source had been optimized by use of finite element analyses (FEA) in order to get an adequate electrical resistance as well as a homogeneous temperature distribution and a minimum deflection of the radiating element. Due to its excellent thermal isolation from the heat sink, the electrical power consumption is very low. Operating temperatures of up to 1400 K are possible, so that the fabricated IR source features a very high radiant power. Its application in gas analysis will improve the performance and efficiency of gas measurement systems.

1 Introduction

Explosion hazards mostly arise from flammable gases and vapors. Instead of avoiding their ignition by explosion protection measurements, it may be preferable to detect them before they become ignitable. Depending on the application, different measuring principles for the detection of gases and vapors can be used, e.g., electrochemical sensors (Bakker, 2004), semiconductor sensors (Capone et al., 2004), and point or open-path infrared gas detectors (Goode et al., 1999). Optical gas detection by use of infrared radiation (IR) is the leading technique in terms of accuracy, reliability, and economic efficiency. Since most gas measurements are made in the two wavelength ranges of (3 . . . 5) and (8 . . . 14) µm, a broadband IR source with a near-blackbody emission characteristic is necessary. For reliable measurements, the generation of a stable spectrum of infrared radiation is crucial. Very low detection limits can be realized by a long optical path, where more gas molecules are involved in the IR absorption, but this requires a very powerful IR source. According to Planck's law of thermal radiation, the spectrum of a thermal emitter with a blackbody characteristic depends only on its temperature T (Howell et al., 2010). The totally emitted radiant power P_S is given by the Stefan–Boltzmann law

$$P_S = \varepsilon \sigma A_{emit} T^4 \quad (1)$$

with emissivity ε, Stefan–Boltzmann constant σ, and the radiating area A_{emit}. Consequently, a high radiation power is mainly realized by a high operating temperature of the thermal emitter, but also by a high and wavelength-independent emissivity of infrared radiation. Especially portable gas sensing devices require a low energy consumption of the IR source. For this reason, the radiating element has to be optimized regarding an excellent thermal isolation.

2 Design and technology

In Schossig et al. (2010) and Schossig (2012), we reported on a novel IR absorber based on a nanostructured NiCr alloy that features a very high and spectrally homogeneous absorptivity. From Kirchhoff's law (Howell et al., 2010),

$$\alpha(\lambda, T) = \varepsilon(\lambda, T), \quad (2)$$

it is known that for the maintenance of thermal equilibrium, the absorptivity α at wavelength λ and temperature T must be equal to the emissivity ε. Therefore, good absorbers are also

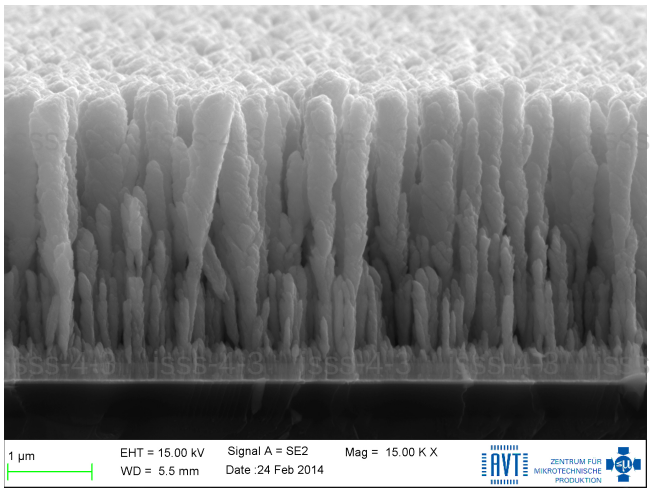

Figure 1. SEM (scanning electron microscopy) picture of a nanostructured NiCr absorber.

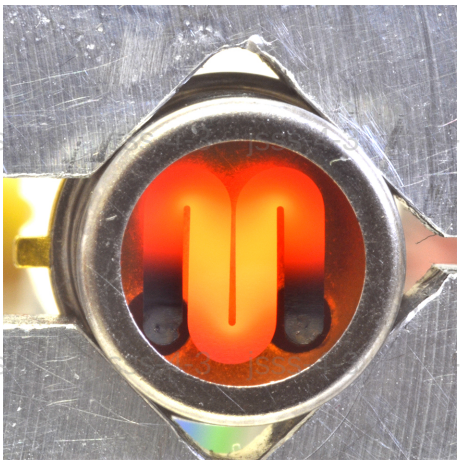

Figure 2. First prototype of a thermal infrared emitter with a nanostructured high-emissivity layer operating at about 1170 K.

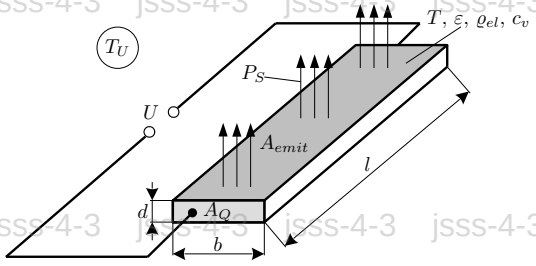

Figure 3. Physical dimensions and boundary conditions of a simplified heating conductor.

good emitters. Since NiCr is one of the most used materials in heating elements, for instance in toasters and hairdryers, we studied the application of the nanostructured NiCr absorber (Fig. 1) in thermal infrared emitters to increase their emittance. By depositing the nanostructured NiCr layer on a thin NiCr foil, the high-temperature stability of the nanostructures could be verified with a first prototype of a thermal IR emitter in a TO-39 package (Fig. 2). Thereby, operation in air causes an oxidation of the surface. The speed of oxidation and the thickness of the oxide are increased with increasing temperature. As a consequence, the spectral emissivity of the nanostructured surface is affected. In contrast, an operation in an inert gas atmosphere does not change its optical properties even at very high temperatures. The layout of the first prototype had some disadvantages. First, it had a very low electrical resistance of about 1 Ω, which is not practicable to use. In addition, the temperature distribution was not homogeneous, as can be seen from Fig. 2. Finally, it had a relatively high power consumption of about 5 W due to the poor thermal isolation of the radiating element.

3 Layout of an ideal heating conductor

As already mentioned, an ideal thermal emitter should feature a high electrical resistance and a low heat capacity (also referred to as thermal mass) in order to be modulated electrically. Furthermore, most of the electrical input power should be transformed into radiant power. This can be achieved by a good thermal isolation, a high emissivity near 100 % and a high average temperature of the emitting area. The emissivity and the average temperature, however, do not have any effect on the shape of the heating conductor. So the focus is on improving thermal isolation and electrical resistance. A simplified current-carrying heating conductor is shown in Fig. 3. In order to improve its geometric shape, the theoretical dependencies need to be considered.

The electrical resistance R of a rectangular conductor is

$$R = \varrho_{\mathrm{el}} \frac{l}{A_Q} = \varrho_{\mathrm{el}} \frac{l}{b\,d}, \tag{3}$$

where ϱ_{el} is the specific electrical resistance of the conductor material and l is the conductor length. The cross section A_Q is the product of conductor thickness d and its width b. As given by Eq. (1), the radiant power is proportional to the emitting area A_{emit}; thus,

$$A_{\mathrm{emit}} = b\,l \tag{4}$$

should be maximized. The conductor material is NiCr. To achieve a high resistance and maximize the emitting area corresponding to Eqs. (3) and (4), the conductor layout can be optimized as follows.

1. Choose conductor length l as large as possible.
2. Minimize cross section A_Q by reducing conductor thickness d, because a smaller conductor width b cuts down on the emitting area.

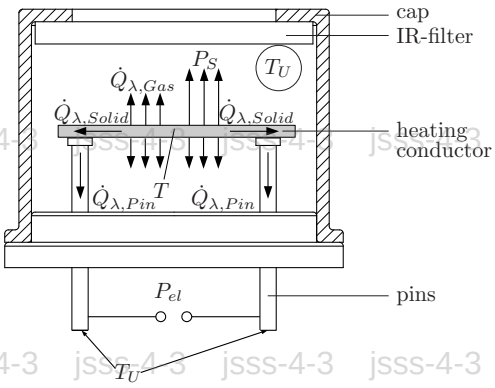

Figure 4. Input power and dissipated heat fluxes of the emitter in the TO-39 housing. For simplification, convection is neglected.

Further requirements for thermal emitters are a high modulation depth m_f (see Sect. 5 for further explanation) and low thermal losses, which can be described with thermal conductance. The thermal conductance G_λ is proportional to the conductor's cross section (Baehr and Stephan, 2011, p. 6):

$$G_\lambda \propto A_Q. \tag{5}$$

The modulation depth is defined here by the ratio of the achievable temperature difference under electrical modulation with frequency f_m vs. the maximum temperature difference without modulation at approximately direct current

$$\mathrm{m}_f = \frac{\Delta T(f_\mathrm{m})}{\Delta T(f_\mathrm{m} \to 0)}. \tag{6}$$

Due to its thermal inertia, the heating conductor requires a certain amount of time to reach the equilibrium temperature after it is turned on. If the modulation frequency is too high, the emitter is not able to reach its equilibrium temperature any more. Thus, the temperature difference $\Delta T(f_\mathrm{m})$ and therefore modulation depth m_f decrease.

The thermal model by Schulz et al. (2005) is used to understand the dynamic heating and cooling of the emitter under cyclic excitation. The model describes these thermodynamic processes analytically. Figure 4 shows the heating conductor in the TO-39 housing. The input power P_el is transformed completely into Joule heat. This heat is dissipated into the environment through

- radiation P_S,
- solid-state heat conduction within the heating conductor ($\dot{Q}_{\lambda,\mathrm{Solid}}$) and the header pins ($\dot{Q}_{\lambda,\mathrm{Pin}}$), as well as
- heat conduction ($\dot{Q}_{\lambda,\mathrm{Gas}}$) through the filling gas.

These dissipated heat fluxes will be collectively referred to as $\dot{Q}_\mathrm{diss}$ subsequently. To describe the thermodynamic behavior of the arrangement, the heat capacity C_th needs to be considered additionally. For the system, the first law of thermodynamics (Baehr and Stephan, 2011, p. 108) applies:

$$\frac{\mathrm{d}U}{\mathrm{d}t} = P_\mathrm{el} - \dot{Q}_\mathrm{diss}. \tag{7}$$

The change in the internal energy $\mathrm{d}U/\mathrm{d}t$ can be described with the heat capacity C_th as follows (Baehr and Stephan, 2011, p. 109):

$$\frac{\mathrm{d}U}{\mathrm{d}t} = C_\mathrm{th}\frac{\mathrm{d}\Delta T}{\mathrm{d}t}, \tag{8}$$

where

$$\Delta T = T - T_U. \tag{9}$$

By inserting Eq. 8 into Eq. 7, the rewritten balance equation results:

$$\frac{\mathrm{d}\Delta T}{\mathrm{d}t} = \frac{P_\mathrm{el} - \dot{Q}_\mathrm{diss}}{C_\mathrm{th}}. \tag{10}$$

If the dissipated heat flux and the input power are not modified, the heating and cooling speed is faster the lower the heat capacity of the conductor is. In consequence, the reduction of the heat capacity C_th increases the modulation depth:

$$C_\mathrm{th} \downarrow \Rightarrow \mathrm{m}_f \uparrow. \tag{11}$$

The conductor's heat capacity C_th is given by

$$C_\mathrm{th} = l\,b\,d\,c_v, \tag{12}$$

where c_v is the volume-specific heat capacity.

Considering the given objective on modulation depth and thermal losses, the following conclusions result.

- To ensure a low thermal conductance for a given conductor's width b, the element thickness d should be as small as possible.
- A small element thickness beneficially leads to a low thermal mass.

In conclusion, a low element thickness yields to high electrical resistance, high modulation depth and low thermal losses. The emitting area is maximized by increasing the conductor's length and width. Regarding the layout, an ideal heating conductor is as thin, as long and as wide as possible. In consequence we choose a thin and long spiral to come as close as possible to an ideal conductor shape.

4 Finite element analysis of heating conductors

To evaluate the quality of a thermal emitter, further criteria must be analyzed. Thermal emitters are optical devices, so the heating conductor needs to stay in focus while under thermal load, meaning a low deflection is required. Furthermore,

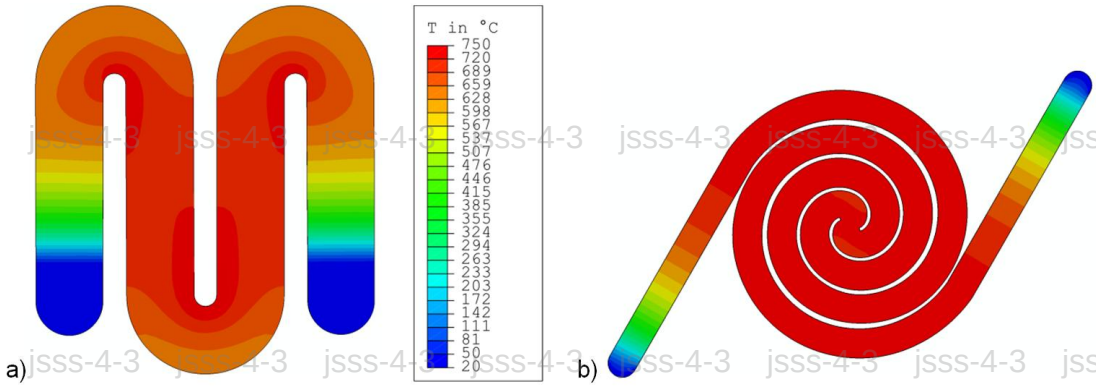

Figure 5. Temperature distribution of **(a)** meander-shaped and **(b)** spiral-shaped emitters.

the mean element temperature directly affects the emitted radiant power. So temperature should be evenly distributed, leading to a high mean temperature. To assess these characteristics, finite element analyses (FEA) have been carried out. The goal is to compare meander-shaped (Fig. 5a) and spiral-shaped conductors (Fig. 5b) with respect to electrical resistance, temperature distribution and out-of-plane deflection (called displacement in FEA).

The boundary conditions for the FEA are the following.

- Thermal: heat sink with $T_U = 20\,°C$ at the pins of the TO39 header;
- electrical: voltage U at the pins;
- optical: emissivity $\varepsilon_{top} = 0.9$ of the top surface (with NiCr nanostructures) and $\varepsilon_{bottom} = 0.3$ of the bottom surface (blank metal); and
- mechanical: fixed support at TO39 pins.

NiCr is used as material. As already mentioned, it can be assumed that all of the electrical input power is transformed into Joule heat.

Table 1 shows the results of the analyses. The temperature distribution of the meander-shaped emitter (Fig. 5a) reproduces the visual appearance shown in Fig. 2, where hotter areas are brighter. Compared to the meander shape, the spiral-shaped element has far more electrical resistance as well as a uniform temperature distribution (Fig. 5b). This leads to a higher mean temperature of the spiral, although the maximum element temperatures of both layouts are equal. Due to the higher mean temperature, the spiral-shaped conductor is twice as efficient as the meander-shaped conductor regarding emitted radiant power. The fixed support of the conductor ends forces the elements to buckle under thermal load. Fig. 6 shows the meander displacement as a result of buckling. After a longer period in operation, we discovered malfunction of the emitter caused by buckling (Fig. 7), which is not tolerable. The magnitude of the spiral displacement is much lower ($u < 0.3$ mm), and tolerable.

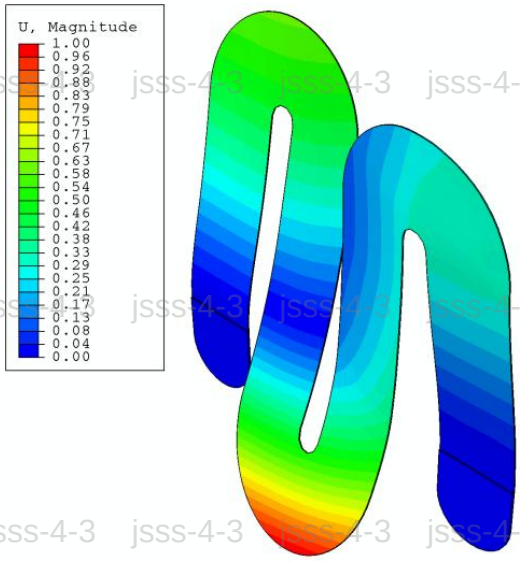

Figure 6. Displacement (deflection) of the meander in mm.

5 Experimental results

New prototypes were fabricated that have the spiral shape. By reducing the thickness of the radiating element to about 10 µm, a direct electrical modulation of the emitted radiation becomes possible. This is an important feature for its application in gas sensing devices because the most commonly used pyroelectric IR detectors are only sensitive to AC signals. Accordingly, it eliminates the use of a mechanical chopper for radiation modulation and, therefore, enables miniaturization and allows for more compact gas sensing devices. The spiral radiating elements were fabricated by ion beam etching of a thin NiCr foil and have a radiating area of about 2.8 mm^2. Both sides are coated with a 2 µm thick nanostructured layer of high emissivity (Fig. 8). The radiating elements are hermetically sealed into common TO-39 housings with a krypton atmosphere (Fig. 9). In order to use the backside-emitted

Table 1. Comparison of meander-shaped and spiral-shaped heating conductors (results of FEA).

	Meander	Spiral
Resistance R	1Ω	30Ω
Emitting area A_{emit}	ca. 16 mm^2	2.8 mm^2
Maximum temparature T_{max} of emitting area	750 °C	750 °C
Mean temperature T [a]	630 °C	720 °C
Electrical input power P_{el} for T	3 W	0.4 W (see Fig. 11)
Radiant power P_S [b]	724 mW	185 mW
Efficiency P_S/P_{el}	24 %	46 %
Displacement u at T	> 1 mm (malfunction)	< 0.3 mm

[a] Calculated with volume-weighted element temperatures.
[b] Calculated with $P_S = (\varepsilon_{top} + \varepsilon_{bottom})\,\sigma\,A_{emit}T^4$ where $\varepsilon_{top} = 0.9$ and $\varepsilon_{bottom} = 0.3$.

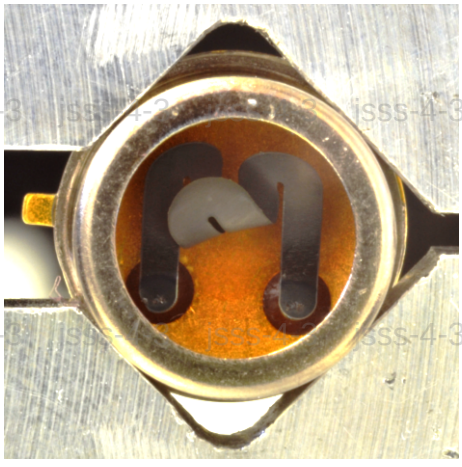

Figure 7. Malfunction of the meander-shaped emitter caused by buckling.

Figure 9. Prototype of a thermal infrared emitter with the near-blackbody emission characteristic in TO-39 housing.

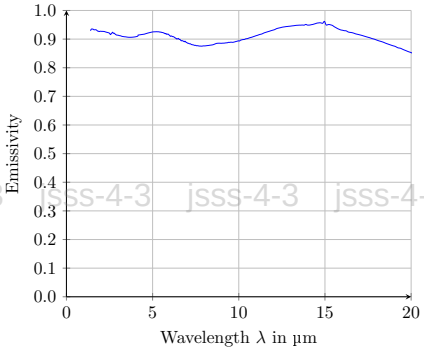

Figure 8. Measured spectral emissivity of the novel thermal infrared emitters with spiral filament.

radiation, a reflector is integrated into the TO-39 housing. In this way, a 70 % higher signal was achieved.

The electrical and optical properties of the new prototypes were studied. We found an adequate electrical cold resistance of about 31Ω ± 3Ω and a slightly higher hot resistance of about 33Ω ± 3Ω (Fig. 10). Accordingly, the emitters can be operated at 3.3 V, a common voltage used in portable devices. In this case, the mean electrical power consumption is 330 mW ± 20 mW, with an operating temperature of 970 K (Fig. 11). For temperature measurement the spectral radiance has been measured with a monochromator as can be seen in Fig. 13. Then the maximum of the spectral radiance has been determined and converted into a temperature with Wien's displacement law. The temperature error is estimated at ±30 K. Comparable thin-film emitters reach only a maximum temperature of about 800 K at the same electrical input power (Micro-Hybrid Electronic GmbH, p. 5).

The thin and low-mass radiating element allows the IR source to be modulated electrically. By applying a square-wave voltage, the emitter is switched on and off. Because a non-contact and fast measurement of the temperature of the electrically modulated source is not possible at the moment, the emitted radiant flux Φ is measured with a broadband and fast IR detector. Another advantage of this approach is the possibility to compare the emitter with commercial IR sources, e.g., from Micro-Hybrid Electronic GmbH and Axetris AG. The frequency response measured with the radiant

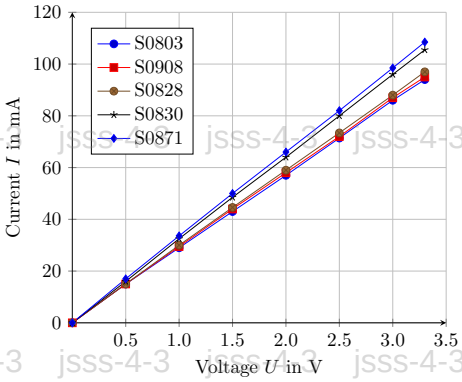

Figure 10. Measured current-voltage characteristic of the IR emitter from Fig. 9.

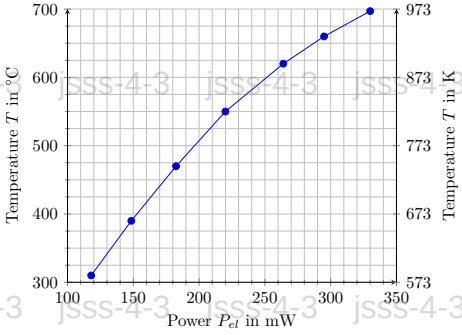

Figure 11. Measured operating temperature in dependence on the electrical power for the IR emitter from Fig. 9.

flux is called normalized optical emission (NOE):

$$\mathrm{NOE} = \frac{\Delta\Phi(f_\mathrm{m})}{\Delta\Phi(f_\mathrm{m} \to 0)}. \quad (13)$$

With increasing frequency, NOE decreases due to the thermal inertia of the emitter. Consequently, the frequency response has a low-pass characteristic (Fig. 12). The measurement results show a maximum modulation frequency of about 3 Hz for 50 % NOE. This is sufficient for most applications. However, the NOE and the modulation depth can be simply increased by a further reduction of the thermal mass.

Finally, the measurement results of the spectral radiance validate the near-blackbody emission characteristic of this thermal infrared source (Fig. 13).

6 Conclusion and outlook

In this paper, we presented a novel thermal IR emitter for application in optical gas detection. It features a very high radiant power, near-blackbody emission characteristic and can be modulated electrically. Due the excellent thermal isolation from the heat sink, the electrical power consumption is very low. This enables an application in portable gas sensing devices. Since the used NiCr alloy allows a permanent

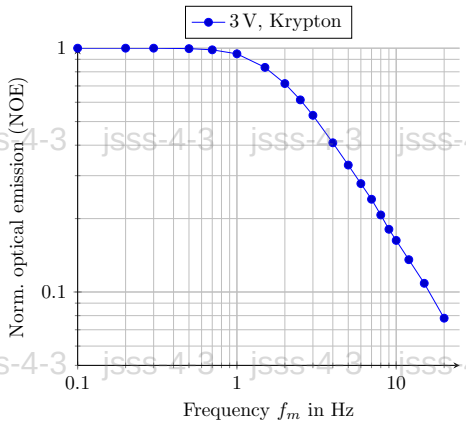

Figure 12. Measured frequency response of the emitter for a constant voltage square-wave drive.

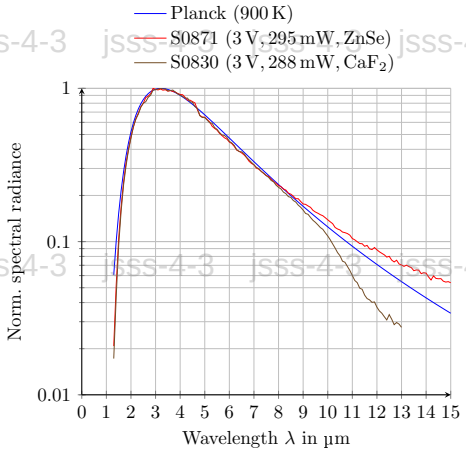

Figure 13. Comparison of the measured spectral radiance of the novel IR source and a blackbody radiator of the same temperature.

operation at temperatures of up to 1400 K, the fabricated IR source should feature a long-term stable performance and a long lifetime. Finally, its application in gas analysis will improve the performance and efficiency of gas measurement systems. Further improvements will target the reduction of the thermal mass of the radiating element in order to increase its modulation depth.

Acknowledgements. The authors would like to thank the German Research Foundation (DFG) for supporting this work under grant number GE 779/32.

Edited by: W. A. Minkina
Reviewed by: two anonymous referees

References

Axetris AG: Infrared Source EMIRS50, available at: https://static.axetris.com/-/media/downloads/400axag/infraredsources/fl-infraredsourceemirs50_en.pdf (last access: 31 August 2015), 2014.

Baehr, H. and Stephan, K.: Heat and Mass Transfer, Springer Berlin Heidelberg, 737 pp., doi:10.1007/978-3-642-20021-2, 2011.

Bakker, E.: Electrochemical Sensors, Anal. Chem., 76, 3285–3298, doi:10.1021/ac049580z, 2004.

Capone, S., Forleo, A., Francioso, L., Rella, R., Siciliano, P., Spadavecchia, J., Presicce, D. S., and Taurino, A. M.: Solid State Gas Sensors: State of the Art and Future Activities, ChemInform, 35, 1335–1348, doi:10.1002/chin.200429283, 2004.

Goode, J. G., Yokelson, R. J., Susott, R. A., and Ward, D. E.: Trace gas emissions from laboratory biomass fires measured by open-path Fourier transform infrared spectroscopy: Fires in grass and surface fuels, J. Geophys. Res.-Atmos., 104, 21237–21245, doi:10.1029/1999JD900360, 1999.

Howell, J. R., Siegel, R., and Menguc, M. P.: Thermal Radiation Heat Transfer, CRC press Taylor & Francis, 5th edn., Boca Raton, p. 61, doi:10.1002/zamm.201290025, 2010.

Micro-Hybrid Electronic GmbH: INFRARED COMPONENTS & SYSTEMS – Micro-Hybrid Product Catalog 2014/2015, available at: http://finder.micro-hybrid.de/fileadmin/user/IR-systems-documents/Micro-Hybrid_IR_Katalog_s.pdf (last access: 27 August 2015), 2014.

Schossig, M.: Optical Absorption Layers for Infrared Radiation, in: Bio and Nano Packaging Techniques for Electron Devices: Advances in Electronic Device Packaging, edited by: Gerlach, G. and Wolter, K., chap. 18, 355–381, Springer Berlin Heidelberg, doi:10.1007/978-3-642-28522-6, 2012.

Schossig, M., Norkus, V., and Gerlach, G.: Infrared Responsivity of Pyroelectric Detectors With Nanostructured NiCr Thin-Film Absorber, Sensors Journal, IEEE, 10, 1564–1565, doi:10.1109/JSEN.2010.2046162, 2010.

Schulz, O., Müller, G., Lloyd, M., and Ferber, A.: Impact of environmental parameters on the emission intensity of micromachined infrared sources, Sensor. Actuat. A-Phys., 121, 172–180, doi:10.1016/j.sna.2004.12.010, 2005.